Corrosion of C-Steel in the Red Sea: Effect of Immersion Time and Inhibitor Concentration

Aisha H. Al-Moubaraki[1,], Awatif Al-Judaibi[2], Maryam Asiri[1]*

[1] King Abdulaziz University, Sciences Faculty for Girls, Chemistry Department
Jeddah, Saudi Arabia.
[2] King Abdulaziz University, Sciences Faculty for Girls, Biological Science Department, Microbiology
Section, Jeddah, Saudi Arabia.
[*]E-mail: ahm13988@hotmail.com; aamaljudaibi@kau.edu.sa

The effect of immersion time and inhibitor concentration on the corrosion of C-steel in Red Sea Water was studied using chemical and electrochemical techniques. Weight loss data revealed that the corrosion rate expressed as pit depth ($\mu m\ year^{-1}$) is time dependent and obeys the power-law equation $P_d = Kt^n$. Kinetic parameters indicate that the corrosion of C-steel occurs under mixed control of diffusion and charge transfer processes. The corrosion forms and corrosion products on C-steel were described under different conditions of immersion periods. The addition of Dill seeds aqueous extract (DSAE) reduces the corrosion rate of C-steel in Red Sea Water effectively. It was found that the inhibition efficiency increases with increasing DSAE concentration and the optimal concentration is about 10%. Electrochemical measurements showed that DSAE acts as a mixed-type inhibitor, without altering the mechanism of C-steel dissolution. Inhibition mechanism of DSAE on the C-steel surface was interpreted based on its effective constituents. The effect of DSAE concentration on microbial growth was also studied and discussed in view of its inhibitory action.

1. INTRODUCTIO

Sea water covers more than 70% of the Earth's surface and is considered the most abundant natural electrolyte. Most metallic materials exposed to sea water are destroyed, due to corrosion [1]. For many engineering materials, sea water is considered the most corrosive of all naturally occurring electrolytes. The most significant parameters that determine seawater corrosivity are the content of dissolved oxygen, temperature, flow rate, salinity and pH. Other factors that determine corrosivity are biological activity (bio-deposits), and the environmental zone of exposure [2,3].

The corrosive effect of sea water has gained increased attention during the last few decades because of offshore exploration of oil and gas. Corrosion is a major problem in desalination plants. In parts of the world with short supply of fresh water, there is an increasing use of sea water for fresh water production [4].

Most metal structures used in sea water (ships, oil platforms, piers, pipelines, etc.) are traditionally made of mild low-carbon and low alloy steels and are subject to corrosion, especially if unprotected. Over the years, there have been reports on the corrosion of steel and its alloys in sea water environments [5-9]. However, no report is available on the corrosion behavior and corrosion kinetic of steels in Red Sea Water. Therefore, the current research sheds light on the corrosion behavior of steel in the Red Sea. The Red Sea is a semi-enclosed tropical body of water located between the Mediterranean Sea and the Indian Ocean, and is bordered by Egypt, Sudan, Eritrea and Djibouti to the west, with Yemen and Saudi Arabia on the east. Although the Red Sea is known for its natural beauty, with extensive coral reefs, it is also an important shipping route for oil tankers and other ships traveling through the Suez Canal [10]. There is an extensive demand for desalinated water to meet domestic and industrial needs along the Red Sea. Thus, there are at least 18 desalination plants along the Red Sea coast of Saudi Arabia [11]. Water from the Red Sea is also utilized by oil refineries and cement factories for cooling purposes. The major industries in the Red Sea region include oil exploration, oil production, oil processing, manufacturing industries (fertilizers, chemicals, cement), tourism, fisheries and oil related maritime transport [10].

Figure 1. The seeds of *Anethum graveolens* L. (Dill).

There are various methods of preventing corrosion, ranging from techniques that separate metals from corrosive environments to environmental modification strategies. One of these methods applies corrosion inhibitors such as polyhydric alcohol phosphate ester [12], sodium nitrite [13], dehydroabietylamine schiff base derivative, namely 2-((dehydroabietylamine) methyl)-6-

methoxyphenol [14], aqueous extract of henna leaves [15], *phyllanthus amarus* extract [16] etc. These materials have been reported as good inhibitors of steel corrosion in sea water.

Anethum graveolens L., commonly known as dill (also known as Shapt), is an annual medicinal plant with tiny yellow flowers belonging to the plant family *Apiaceae* (*Umbelliferae*). The genus name *Anethum* is derived from the Greek word aneeson or aneeton, which means strong smelling. The plant grows in Pakistan, India, Afghanistan, Middle East, Russia, Iran and Egypt [17]. Its seeds (Fig.1) have a strong spicy odor and are therefore used as a flavoring agent in the food industry. Dill seeds are commonly used in the treatment of aches in the stomach and intestines, dyspepsia, bladder inflammation, liver diseases, cramps, and insomnia. The essential oil and extracts of dill seeds have shown varying degrees of antimicrobial activities [18].

This research studied the corrosion of C-steel in Red Sea Water through:

➢ The effect of immersion time on corrosion behavior of C-steel in Red Sea Water and by identifying corrosion forms and the corrosion products after different immersion periods.

➢ The effect of dill seeds aqueous extract (DSAE) on the corrosion of C-steel in Red Sea Water after a specific time of immersion (5 weeks).

2. EXPERIMENTAL

2.1. Specimens and Surface Pretreatment

Table 1. Percentage composition of the studied specimens.

C	Si	Mn	P	S	N	Fe
0.28	0.22	0.73	0.015	0.006	0.007	Remainder

The chemical composition of commercial specimens of C-steel used, are as presented in Table 1. The specimens were cut in the form of a small rod, 5.0 cm in length and 1.0 cm in diameter. Before all measurements, the exposed surfaces were polished with different grades of emery papers, starting with a coarse one and proceeding in steps to fine grades. After this process, the specimens were rinsed with double-distilled water, degreased in ethanol, and finally dried with air. The specimens were then weighed and immersed in the test solution.

2.2. Test Solution and Inhibitor

The test solution was natural sea water and it was collected directly from the Red Sea in the western region (Obhur, Jeddah, Saudi Arabia). The geographic location of the sea water sample is as shown in Fig. 2. Several properties of the sample (pH, electrical conductivity, total alkalinity and content of different ions) were determined in accordance with the Standard Methods for the Examination of Water and Wastewater [19], listed in Table 2.
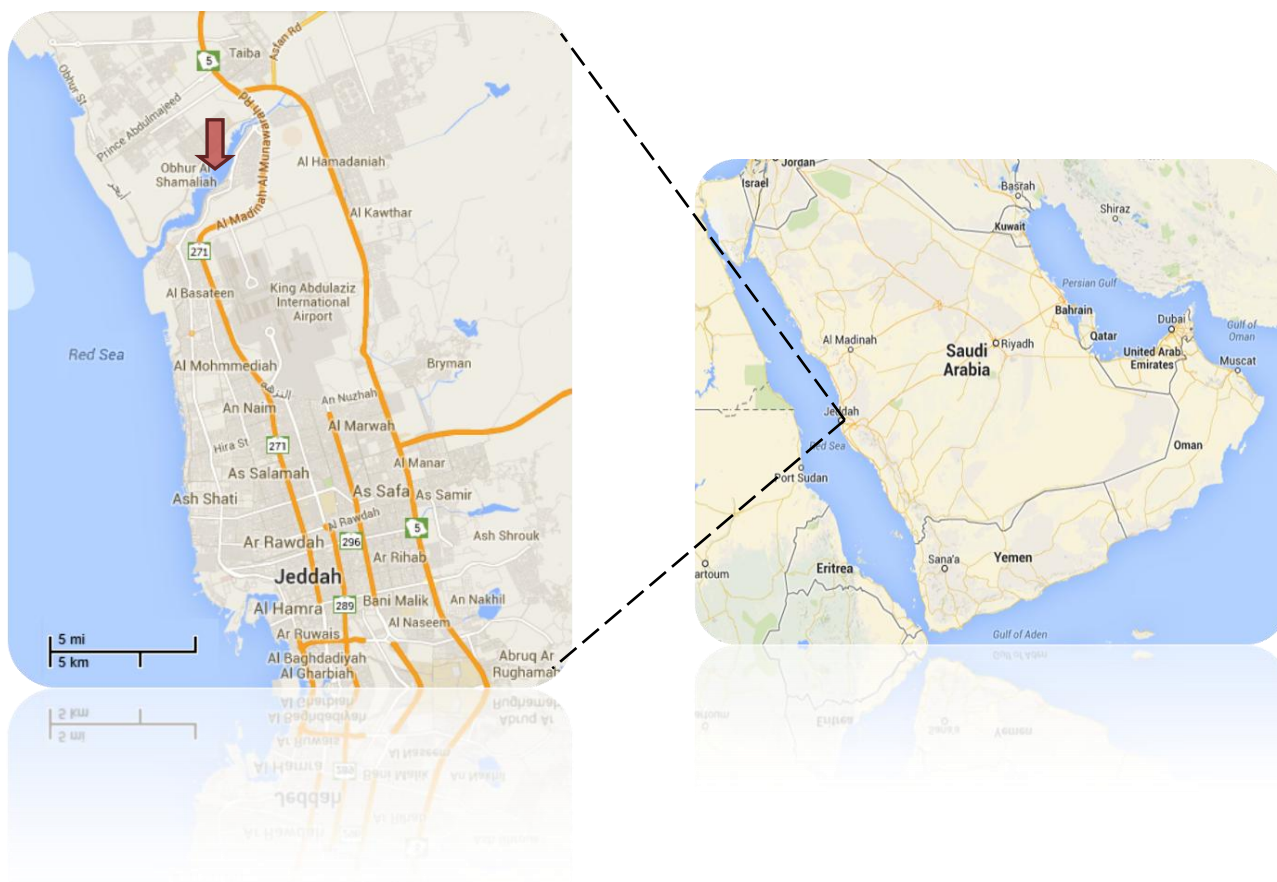
Figure 2. Location of sea water sample collected (arrow) in Jeddah, Saudi Arabia.

Table 2. Chemical analysis of Red Sea Water sample (mg L^{-1}).

Parameter		Value
Salt content (mg L^{-1})	Ca^{2+}	496.0
	Mg^{2+}	1512.0
	Na^{+}	11920.0
	K^{+}	588.0
	Cl^{-}	22336.0
	HCO_3^{-}	156.0
	NO_3^{-}	1.0
	SO_4^{2-}	2440.0
	PO_4^{3-}	< 0.1
	CO_3^{2-}	< 0.1
	SiO_2	< 1.0
	Total dissolved solid (TDS)	43550.0
	Total suspended solids (TSS)	< 5.0
	Total alkalinity	128.0
pH		8.1
Electrical Conductivity (μS/cm)		72550.0

DSAE was used as an inhibitor and a stock solution; it was prepared by boiling 25 g of the dry grounded dill seeds in 500 mL of double distilled water for 2 h. The extract was then filtered to remove suspended impurities, and double distilled water was added to make it up to 500 mL. The concentration of the inhibitor used ranged from 0.5 to 25 mL% (v/v %).

2.3. Corrosion Rate Measurements

The corrosion rate of C-steel in Red Sea Water was assessed using chemical (weight loss (WL)) and electrochemical (potentiodynamic polarization (PDP) and electrochemical impedance spectroscopy (EIS)) measurements as follows:

2.3.1. Chemical Measurements

Polished and pre-weighed C-steel specimens were placed in airtight glass containers containing 100 mL of sea water for different immersion periods (1, 2, 3, 5, 7 and 10 weeks) at an ambient temperature (lab temperature was $21\pm1^{\circ}C$) under stagnant conditions. In order to identify the immersed specimens in various periods, stamped code numbers were used. In case of inhibitor addition, a certain amount of DSAE was mixed with sea water. Then, polished and pre-weighed specimens of C-steel were immersed in the inhibited systems and the corrosion rates were calculated over a 5 week immersion period. At the end of each immersion period, the specimens assessed by weight-loss measurement. Layers of rust were scraped off the steel surface with a bristle brush and immediately immersed in the respective pickling solution for 5 min [20]. After corrosion products had been completely removed, the specimens were rinsed with double distilled water, and ethanol, dried with a stream of air, and reweighed to determine mass loss. Duplicate experiments were conducted for all weight loss experiments.

The corrosion rate (CR) was calculated in μm year^{-1} according to the following equation:

$$\text{CR} \ (\mu m \ \text{year}^{-1}) = \frac{\Delta W}{Adt} \times 10^4 \tag{1}$$

where ΔW is weight loss in grams (g), A is area in square centimeters (cm^2), d is metal density in (g cm^{-3}) and t is the exposure time in year.

The inhibition Efficiency (IE_{WL} (%)) values can be calculated from WL data using the following equation:

$$IE_{WL}\% = (\frac{CR^o - CR}{CR^o}) \times 100 \tag{2}$$

where CR^o and CR are the corrosion rates of C-steel in the absence and presence of a certain concentration of inhibitor, respectively.

2.3.2. Electrochemical Measurements

Electrochemical measurements were performed in a three electrode cell, A C-steel specimen was used as the working electrode, a platinum wire as the counter electrode and silver/silver chloride (Ag/AgCl$_{(s)}$/KCl$_{saturated(aq)}$) as the reference electrode.

Prior to the electrochemical measurements, the working electrode was treated as earlier described and immersed in the sea water test solution. The EIS measurements were performed at open circuit potential, after 1 h of immersion in the test solution. During EIS measurements, an AC disturbance signal of 10 mV was applied on the electrode. The measuring frequency ranged from 0.1 to 30,000 Hz. The potentiodynamic current-potential curves were carried out by linearly changing the electrode potential from the starting (-1000 mV) potential with respect to SCE towards more less negative direction with the required scan rate (1mV/s) till the end of the experiment (-100 mV). Apotentiostat galvanostat (ACM Gill AC instrument model 1649) was used for the electrochemical measurements. All impedance data were fitted to appropriate equivalent circuits using the computer program ZSimDemo 3.20.

The percentage inhibition efficiency was obtained from polarization resistance and current density values, using Equations 3 and 4 respectively:

$$IE_R\% = (1 - \frac{R_P^o}{R_P}) \times 100 \tag{3}$$

where R_P^o and R_P are the polarization resistance of C-steel in the absence and presence of a certain concentration of inhibitor, respectively.

$$IE_i\% = (1 - \frac{i_{corr}}{i_{corr}^o}) \times 100 \tag{4}$$

where i_{corr}^o and i_{corr} are the corrosion current densities of C-steel in the absence and presence of a certain concentration of inhibitor, respectively.

2.4. Surface Examination Study (Optical Photograph)

Optical photographs of the C-steel specimens were taken after the chemical and electrochemical experiments to evaluate gross changes in the metal surface and to perform a cursory evaluation of the forms of corrosion (e.g., general, pitting, etc.) at different conditions. Optical photographs were taken using VMS-004 USB microscope.

2.5. Microbial Analysis (Under Aerobic Condition)

Sabouraud dextrose agar (SDA) was used as the medium with an OXOID code of CM41 [21]. This medium has an acid pH for the isolation of yeast if present.

Nutrient agar was used as a medium with an OXOID code of CM3 [22].

Thiobacillus sp. was cultivated in thiosulfate medium with the following composition (per L): 10.0 g of $Na_2S_2O_3.5H_2O$, 4.0 g of KH_2PO_4, 4.0 g of K_2HPO_4, 1.0 g of NH_4Cl, and 0.4 g of $MgCl_2.6H_2O$, with 0.5 mL of trace element solution added and the pH was 6.7 [21].

The thiosulfate mineral medium had the following composition (g L^{-1}): NH_4Cl (0.1), KH_2PO_4 (0.05), $MgSO_4.7H_2O$ (0.02), $NaS_2O_3.5H_2O$ (0.4), yeast extract (1.0), agar-agar (18), the pH was adjusted to 3 with sulfuric acid [23].

The 9K solid medium was composed of (g L^{-1}): KH_2PO_4 (0.4), $CaCl_2.2H_2O$ (0.2), $MgSO_4.7H_2O$ (0.4), $(NH_4)_2SO_4$ (0.4), $FeSO_4.7H_2O$ (33.3) agar-agar (18). The medium was adjusted to pH 1.5-2 with sulfuric acid [23].

3. RESULTS AND DISCUSSION

3.1. Effect of Immersion Time

3.1.1. Time dependence of Corrosion Rate

Table 3. Pit depth and corrosion rates of C- steel at different immersion times in Red Sea Water.

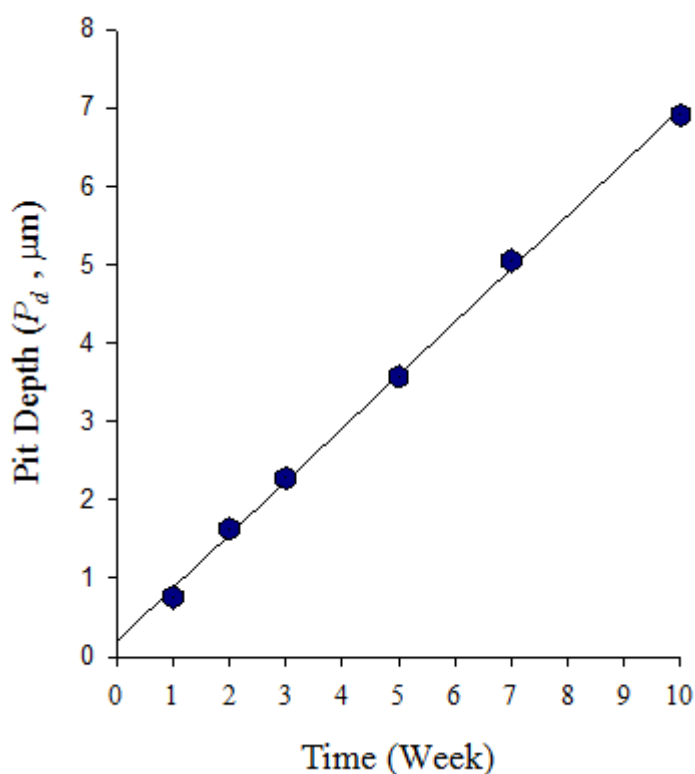| Period of immersion (weeks)	Pit Depth (P_d) (μm)	Corrosion Rate (μm year^{-1})	Current Density (i_{corr}) (μA cm^{-2})
1	0.761	39.84 ± 0.334	3.41 ± 0.040
2	1.633	42.52 ± 0.092	3.66 ± 0.007
3	2.279	39.64 ± 0.785	3.40 ± 0.068
5	3.575	37.28 ± 0.402	3.22 ± 0.062
7	5.055	37.67 ± 0.438	3.25 ± 0.037
10	6.914	36.05 ± 0.064	3.10 ± 0.005

Figure 3. Variation of pit depth of C-steel in Red Sea Water with immersion time.

Weight-loss measurement is the most accurate method of determining metal corrosion rate because the experiment is easy to replicate. Although long exposure times may be involved, the relatively simple procedure reduces the propensity of committing systematic errors.

Corrosion rate, and weight loss of C-steel in Red Sea Water (due to corrosion for a 10 week period) expressed as penetration depth or pit depth are listed in Table 3.

It is clear that pit depth increases linearly with immersion period (Fig. 3) indicating that sea water is highly corrosive toward C-steel under the studied conditions. Sea water contains a high concentration of chloride ions (Cl^-) capable of destroying the passive layer and protective film on C-steel. Long immersion periods increase the exposure of C-steel surface to Cl^- ions, resulting in more weight loss.

The conversion of gravimetric parameters into electrochemical quantities was achieved by means of Faraday's law [24]:

$$i_{corr} = \frac{nF\Delta m}{MAt} \tag{5}$$

where i_{corr} is current density in $A\ cm^{-2}$ which stands for corrosion rate, Δm is weight loss due to corrosion in g, n is valence of Fe, F is Faraday's constant (96,500 coulombs), M is molecular weight of metal in $g\ mol^{-1}$, t is time in s, and A is the area of metallic surface exposed to the corrosive environment in cm^2. Corrosion current densities of C-steel in Red Sea Water are listed in Table 3. It is obvious that corrosion rates and corrosion current densities increase with immersion time then tend to decrease. This result agrees with previous studies [25, 26] on corrosion of steel in different natural environments. The reason for this phenomenon can be described as follows: the corrosion product builds up on the surface, thereby providing an obstruction to the inward diffusion of oxygen and other agents to the metal surface. This results in the slowing down of the kinetics of the cathodic reactions. Therefore, increase in corrosion product thickness decreases corrosion rate [8]. This corrosion product is not truly passivating as it acts as a membrane, especially in the presence of aggressive ions such as the Cl^- ions. If Cl^- ions are present in the aqueous phase, it can penetrate the corrosion product layer and corrode the steel (increase in pit depth value), although at a reduced rate. The corrosion product is usually quickly formed on the steel surface, but it takes a considerably longer time to reach a steady state which is not seen in this study because the times of immersion included in the study are not sufficient to reach steady state.

3.1.2. Kinetic study

The most commonly applied model for predicting deterioration in aqueous (wet) solutions is the power law [27]:

$$P_d = Kt^n \tag{6}$$

where K is the first year pit depth (μm) during the time of exposure t (year) and n is the corrosion constant. The first year corrosion rate is an important parameter not only for sea water corrosivity determination, but also for long-term corrosion forecasting. Both K and n are dependent on the type of metal and sea water parameters. The power law can be derived from the theory of

diffusion of oxygen through the thick corrosion products formed on the metal surface [28-30]. Power law has been used to explain the corrosion of buried pipeline [31, 32, 26], material loss in atmospheric corrosion [33, 34, 25], and for long-pit depth development of major mechanical equipment [35].

This equation can be written in the logarithmic form:

$$\log P_d = \log K + n \; \log t \tag{7}$$

The representation of corrosion data vs. time on log-log coordinates gave points approximately on a straight line of slope 'n', and the intersection of ordinate 'K', for t = 1. Fig. 4 shows the log-log plot obtained and Table 4 shows the values for 'n', 'K' and correlation coefficients 'r^2' for C-steel corrosion in Red Sea Water.
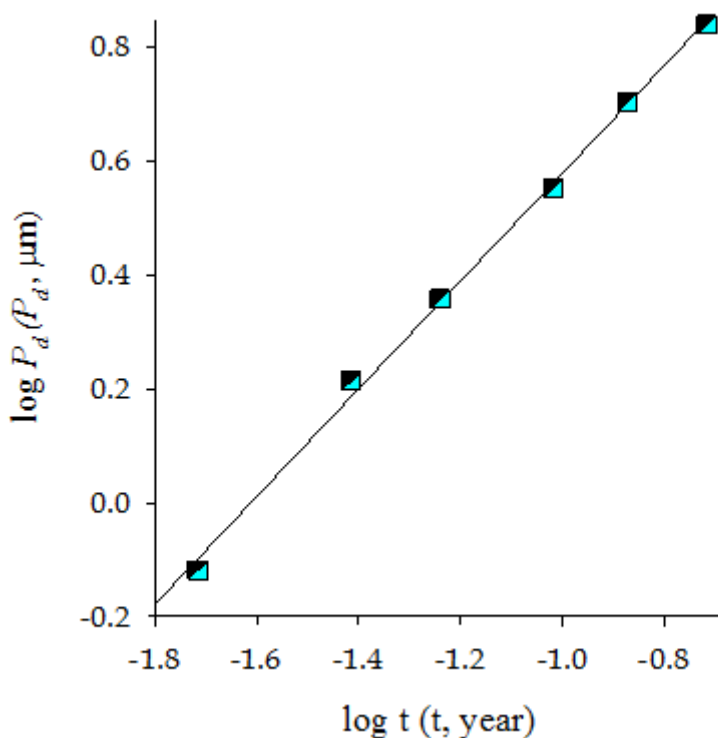

Figure 4. Log P_d as a function of log t for C-steel over ten weeks of immersion in Red Sea Water.

Table 4. Corrosion kinetic parameter of C-steel in Red Sea Water.

Corrosion Kinetic Parameters		
n	K (μm year^{-1})	r^2
0.95	33.57	0.99

The results obtained can be interpreted as follows:

➢ On log-log coordinates, the points lie close to a straight line for C-steel corrosion in Red Sea Water. Thus, it is reasonable to accept verification of the law of power function in estimating long-term corrosion of C-steel. The correlation coefficient 'r^2' for the analysis was very close to unity, indicating an excellent correlation of the data. Additional evidence of the quality of fit is presented in Fig. 5 in which predicted pit depth values (*μm*) were plotted against the corresponding experimental values for C-steel, after different immersion periods. Reasonable agreements between experimental and predicted results were observed.
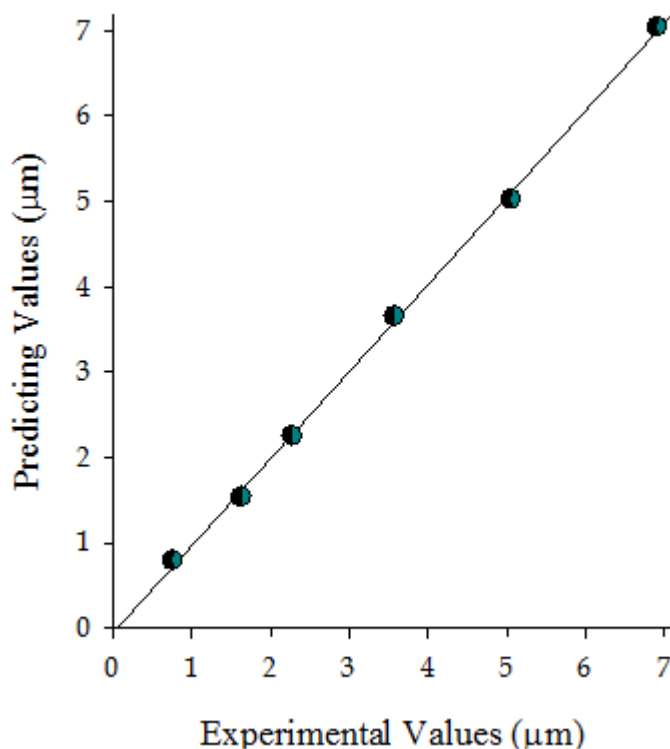

Figure 5. Experimental values vs. predicted values of pit depth (*μm*) of C-steel in Red Sea Water at various immersion periods.

➢ The '*n*' value was about 0.95, suggesting mixed diffusion and charge transfer control mechanisms as well as a gradual change from the diffusion control mechanism to charge transfer control mechanism. This is due to the presence of protective layers of corrosion products which lowered diffusion of corrosive species to the metal surface [25, 26].

➢ The value of '*K*' was equal to the corrosion loss after a first year exposure and indicated vulnerability to rusting, at the beginning of exposure.
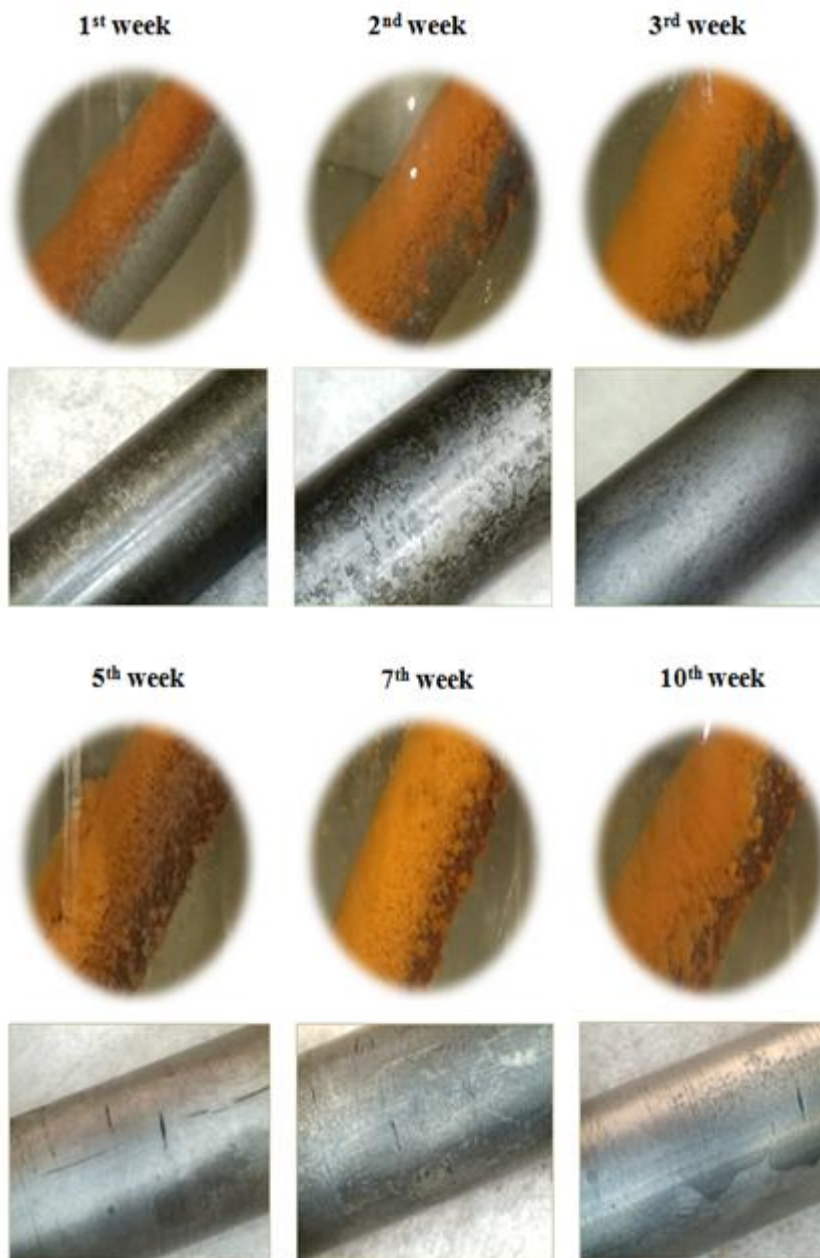
3.1.3. Macroscopic Observations

Figure 6. Visual images of C-steel specimens after immersion in Red Sea Water at different time intervals.

Fig. 6 shows photographs of C-steel specimens before and after they were removed from Red Sea Water, after different immersion periods. The different observations obtained from this figure were attributed to the metal type and can be summarized as follows:

❖ First three weeks of exposure

After one week's exposure, the sample was covered with a thin orange layer of iron oxide (rust). After the sample was cleaned, it was estimated that more than half the surface area showed a distinct cathodic region (dark areas), i.e., areas with no metal loss. While significant metal loss

occurred in the anodic regions. At the end of the second week of exposure, the density of the rust layer increased, as it becomes sponge-like. In the cleaned sample, the large cathodic regions appeared to have started breaking. After three weeks of exposure, the sample was covered with a thick layer of iron oxide. Cleaning revealed a soft black corrosion product layer beneath the oxide layer. There is evidence [36] that the black product consists of magnetite (Fe_3O_4) and iron sulfide (FeS). The cleaned sample showed some distinct cathodic regions remained, but these were smaller than previously, suggesting most had broken up. The sample surface also showed some scratch marks called crevice corrosion.

❖ Exposure from five to ten weeks

Thickness of the rust layer increased, as corrosion products accumulated with increase in immersion time. At the end of five weeks of exposure, the black inner layer grew thicker. The continued corrosion of the surface resulted in marked development of crevice and formation of corrosion products. At this time, there were no clearly identifiable cathodic regions. After seven to ten weeks of exposure, the corrosion product extended to the entire surface, some of which had partially broken away. The black inner layer became thicker as a function of the period of exposure. Apart from the crevices becoming deeper after the seven weeks exposure, irregularly shaped broad pits also emerged after ten weeks of exposure. These broad pits called channel style corrosion were initially small pits before merging into channels. This corrosion pattern can result in defects with significant depth and length.

The aforementioned observations as well as corrosion rates are dependent on the composition of the C-steel sample, environmental conditions (such as water temperature) and the immersion period. The anodic and cathodic regions form very quickly after immersion. In some cases, anodes tend to appear at locations that have high surface energy. The anode/cathode area ratios and locations, once established, change little until the surface is covered by the corrosion product. During this time, observations show that the anodic and cathodic regions were more likely to reduce in size and break up with time. Observations of the formation of anodic and the cathodic regions are not new [30], and there are suggestions about the development of these regions with time. One of these [36] suggested that the cathodic regions reduce in size and break-up, while that the anodic regions tend to spread. This suggestion confirms the observations that were made earlier in this study.

3.1.4. Development of Corrosion with Time

Previous observations on the corrosion of C-steel in Red Sea Water show that corrosion of iron involves the dissociation of ferrous metal to ferrous ions, as expressed in the half-cell reaction:

Anodic reaction

$$Fe \rightarrow Fe^{2+} + 2e^- \tag{8}$$

In a near neutral pH environment, where dissolved oxygen is present (oxic conditions), reduction of oxygen is the predominant cathodic reaction:

Cathodic reaction

$$O_2 + 2H_2O + 4e^- \rightarrow 4OH^- \tag{9}$$

For this, the most immediate common corrosion product is ferrous hydroxide $Fe(OH)_2$ [37].

The overall reaction:

$$2Fe + O_2 + 2H_2O \rightarrow 2Fe(OH)_2 \downarrow \qquad (10)$$

This reaction is accompanied by negative changes in free energy and enthalpy (exothermic). Furthermore, if the local pH within the rust layers is above 7.2 (as is typical in seawater), $Fe(OH)_2$ will oxidize slowly to hydrated magnetite ($Fe_3O_4.xH_2O$) [38] or to one or more mixed valence compounds [39]. In the model of Wranglen [40], rust layers are represented as two layers-an outer $FeOOH$ layer and an inner magnetite layer.
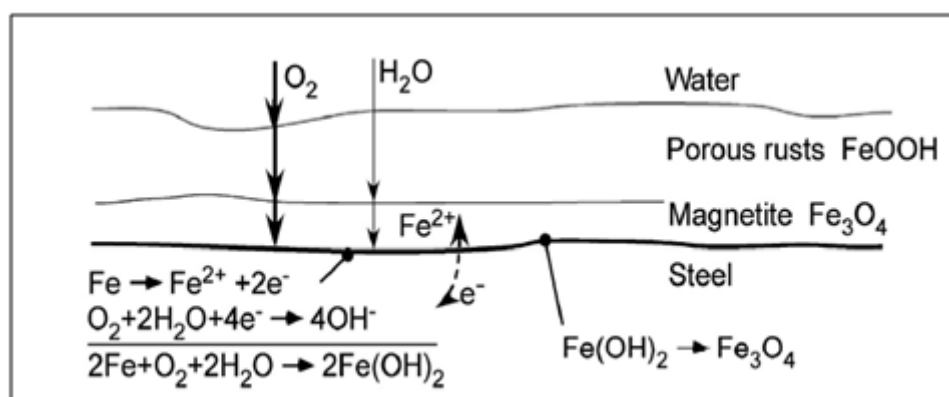
Scheme 1. Reactions involved in corrosion under oxic conditions.

Scheme 1 is a simplified summary of the corrosion reactions that occur under oxic conditions [41].

As the corrosion process continues, corrosion products continue to build-up, increasingly impeding the ability of oxygen to diffuse from the exterior environment to the corroding surface. These conditions lead to the development of localized low oxygen or anoxic conditions on the corrosion interface. Under anoxic conditions, the most likely mechanism is a cathodic reaction involving the dissociation of water, followed by hydrogen reduction with evolution of hydrogen gas [40, 42]:

$$H_2O \leftrightarrow H^+ + OH^- \qquad (11)$$
$$2H^+ + 2e^- \rightarrow H_2 \uparrow \qquad (12)$$

Some studies have documented H_2 formation coupled with iron metal oxidation under anoxic, and near neutral pH conditions [43-45]. These reactions together with the reaction in Eq. (8) can be written as one overall reaction [46]:

$$Fe + 2H_2O \rightarrow Fe(OH)_2 \downarrow + H_2 \uparrow \qquad (13)$$

The precipitated ferrous hydroxide $Fe(OH)_2$ may be oxidized to magnetite Fe_3O_4 or in wet environments to its hydrated form, $Fe_3O_4.xH_2O$ [47]. These reactions occur at a very slow rate under normal low temperature [48]. Under anoxic conditions, crevice and pits develop on steel surface. In his study, Wranglen [40] noted that crevice or pitting corrosion occurred under anoxic conditions. He also stated that the corrosion process was autocatalytic, typically producing a very fast pit or crevice which

grew faster than the general corrosion under anoxic conditions. He emphasized that some of the sulfide inclusions, were active and acted aggressive species in the autocatalytic process. Sulfur in steel usually occurs as inclusions of FeS or MnS. Small amounts are sufficient to have a significant effect on the rate of crevice and pitting corrosion, provided the inclusions are small in size [40]. A relevant chemical reaction is the dissolution of sulfides, as follows:

$$FeS + 2H^+ \rightarrow H_2S + Fe^{2+} \ (or \rightarrow HS^- + H^+ + Fe^{2+}) \tag{14}$$

where H_2S or HS^- is considered the 'aggressive species'.

In chloride rich environments such as sea water (in the present study), the presence of chlorides permits some other reactions. One is the multi-step production of ferrous chloride represented by the equilibrium reaction [49]:

$$Fe^{2+} + 2Cl^- \leftrightarrow FeCl_2 \tag{15}$$

When exposed to air, $FeCl_2$ is readily oxidized to $FeCl_3$ and then to the chloride containing akaganeite ($\beta - FeOOH$) [50] and goethite ($\alpha - FeOOH$) [47]. There are other reactions that involve the production of $FeOCl$ and $Fe_2(OH)_3Cl$ but these intermediates are quickly converted to $\beta - FeOOH$ and $\alpha - FeOOH$ [51, 52]. The morphology, composition and structure of the rust layer formed on C-steel exposed to sea water were analyzed using different methods [53]. The results emphasize Wranglen's model and the role of chloride ions in the corrosion of steel in sea water and concluded that the rust layer can be divided into two layers. An outer rust layer containing lepidocrocite $\gamma - FeOOH$ and an inner rust layer containing mainly $\gamma - FeOOH$, $\alpha - FeOOH$, $\beta - FeOOH$ and Fe_3O_4. In addition, chlorides must enter the pit or crevice from the external environment, if they are to act as aggressive ions in pitting corrosion under anoxic conditions [49, 54].

Under anoxic conditions, it is possible to involve of anaerobic biotic processes, principally involving bacteria. For steel corrosion, this tends to be the obligatory anaerobic sulfate reducing bacteria (SRB) [55]. The most probable process for corrosion resulting from SRB is the biotic production of H_2S [56]. If H_2S diffuses into the pit interior, it will play a role similar to HS^- from abiotic reactions or the 'aggressive ion' HS^- in the reaction of Eq. (14). Thus biotic production of H_2S or HS^- will add to any abiotic HS^- produced from sulfides in the steel, as shown in Eq. (14). The extent to which biotic sulfide ion will increases pitting corrosion, depends on the rate at which it diffuses inwards through the corrosion products.
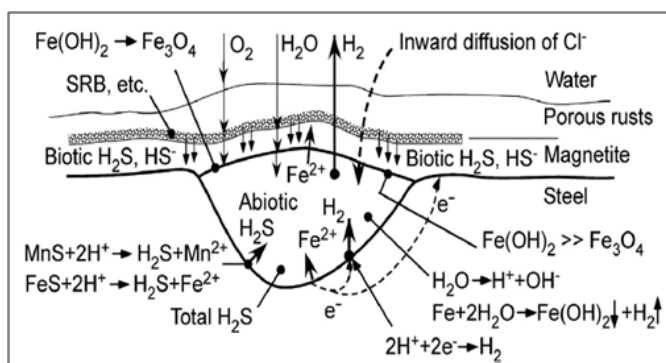
Scheme 2. Sectional view of a typical pit and corrosion products formed in anoxic conditions.

Scheme 2 shows all the reactions involved under anoxic conditions [41].

3.2. Effect of Inhibitor Concentration

3.2.1. Chemical Measurements

Table 5. Corrosion rates and inhibition efficiencies for C-steel in Red Sea Water in the absence and presence of different concentrations of DSAE after five weeks of immersion.

C_{inh} (v/v%)	Pit Depth (μm)	Corrosion Rate (μm year^{-1})	Inhibition Efficiency ($IE_{WL}\%$)
0.0	3.575	37.28 ± 0.402	-
0.5	4.820	50.26 ± 0.605	-34.82
1.0	4.154	43.91 ± 0.844	-17.78
1.5	2.859	29.81 ± 0.249	20.04
2.0	1.763	18.38 ± 0.146	50.70
2.5	1.085	11.31 ± 0.035	69.66
5.0	0.756	7.88 ± 0.307	78.86
10.0	0.479	5.00 ± 0.179	86.59
13.5	0.516	5.38 ± 0.126	85.57
17.5	0.674	7.03 ± 0.081	81.14
25.0	1.079	11.25 ± 0.367	69.82

Corrosion rates and inhibition efficiencies were calculated for C-steel in Red Sea Water and are listed in Table 5. They were calculated from weight loss data in the presence of different concentrations of DSAE, at the experimental temperature. The results can be illustrated as follows:

➢ An acceleration behavior was observed with the addition of low concentrations of DSAE (0.5 and 1.0 v/v%). The accelerating effect of DSAE decreased with increasing concentration. This may be due to decrease in the potential of the cathodic reaction (reduction of oxygen) [57]. Another explanation is that low concentrations of the DSAE were not enough to confer a protective film on the specimen, which would have reduced interfacial reactions between the metal/sea water environment. Low concentrations of DSAE may provide a suitable environment for microbial growth, which promotes C-steel corrosion in Red Sea Water.

➢ In general, pit depth and corrosion rate values decreased gradually, i.e., the corrosion of C-steel was retarded by increase in DSAE concentration.

➢ Inhibition efficiency increased with increase in DSAE concentration, implying a dependence of the inhibitory process on the amount of inhibiting species present in the system. This can be attributed to increased adsorption of DSAE molecules onto the C-steel surface.

➢ Maximum inhibition efficiency for DSAE in Red Sea Water was obtained at a concentration of 10%, after which it started to decrease. This decrease indicates that a concentration of 10 % can be regarded as optimal concentration for this inhibitor. The decrease in inhibition efficiency at inhibitor concentration > 10%, may be caused by decomposition and dissolution of the

protective film on the C-steel surface. This can be attributed to competitive adsorption between DSAE molecules on the metal surface.
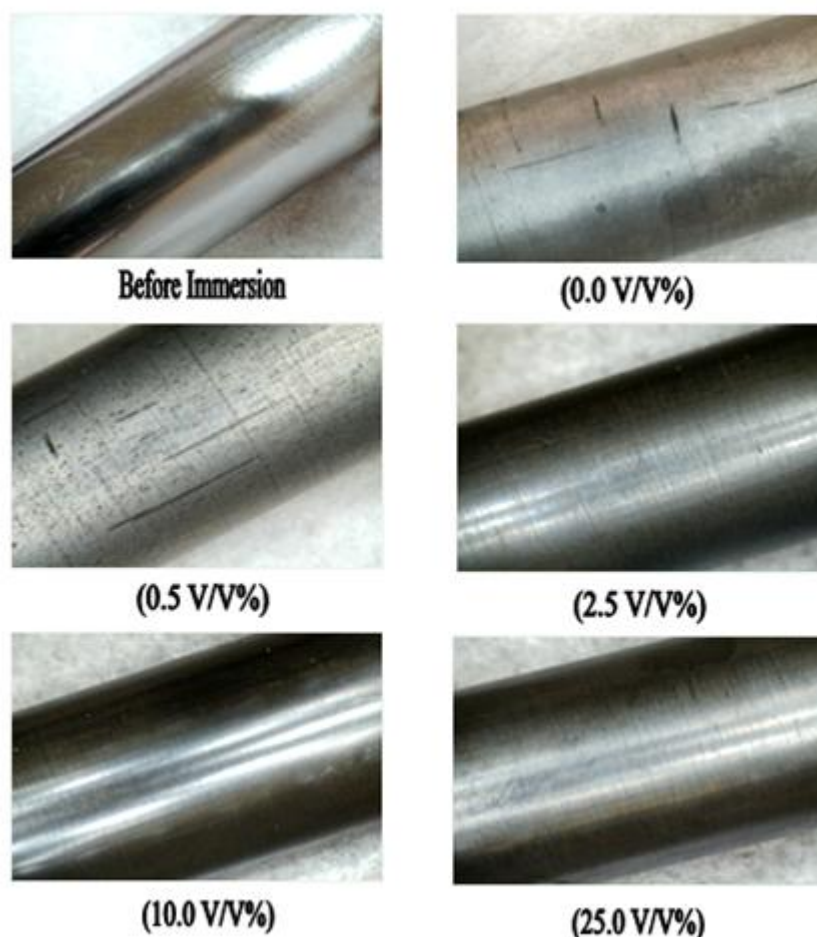

Figure 7. Visual images of C-steel specimens before and after immersion in Red Sea Water for five weeks in the absence and presence of different concentrations of DSAE.

With regard to inhibition, it is generally assumed that inhibitor adsorption at the metal-solution interface, is the first step in the action mechanism of inhibitors in the corrosive media. To establish whether inhibition is due to the formation of an organic film on the metal surface, macroscopic graphs were taken for C-steel specimens in the absence and presence of different concentrations of DSAE (Fig. 7). From the figure, it can be seen that the addition of low concentration (0.5 v/v%) of DSAE accelerates corrosion rate by increasing the formation of crevices and small pits on the C-steel surface. DSAE was more effective at high concentration, as no evidence of crevices or pits were observed on the steel surface. The metal surface was nearly intact at the optimal concentration (10.0 v/v%) and was similar to the original sample before immersion in the aggressive solution. This result indicates that the inhibitor film was modified as the inhibitor concentration increased and adsorption of inhibitory constituents around the crevices and pits may have occurred in the early stage of formation. Increasing

inhibitor concentration more than 10.0 v/v% (optimal concentration), decreases inhibition efficiency, although the sample still remains partially protected.
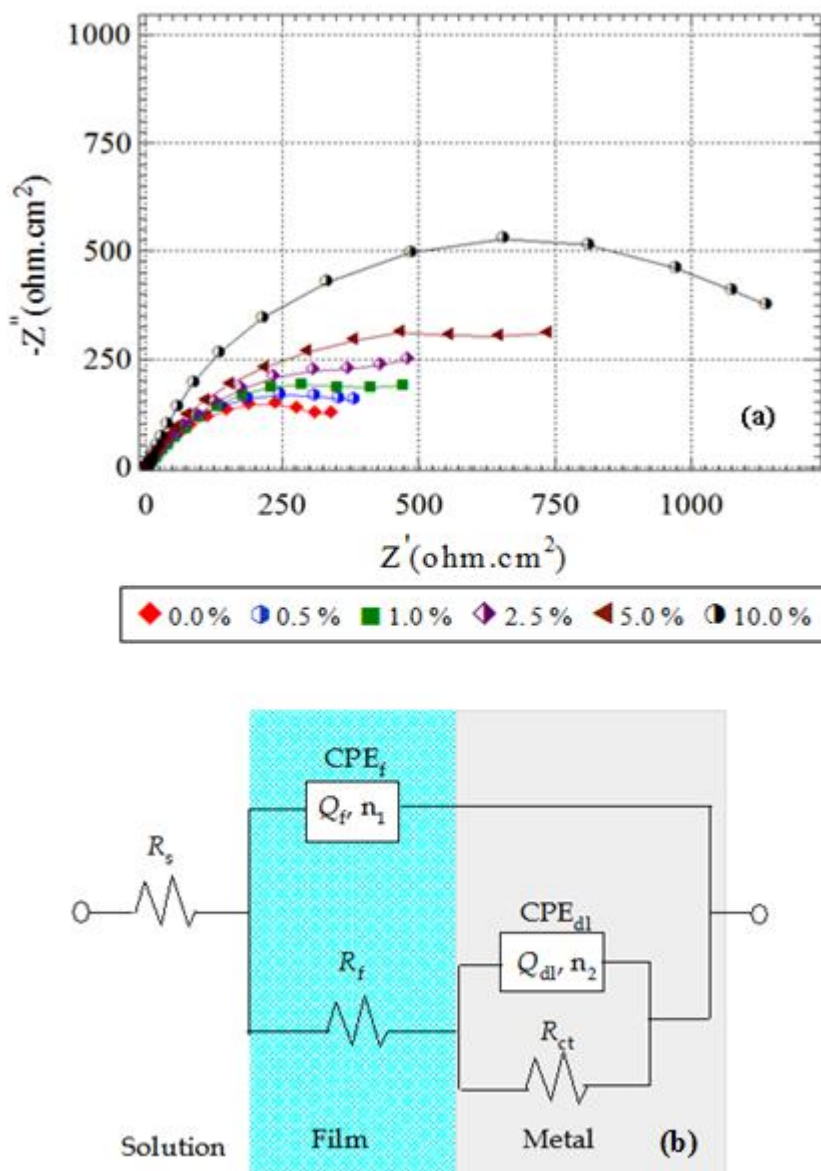
3.2.2. Electrochemical Measurements

Figure 8. (a) Nyquist plot for C-steel in Red Sea Water in the absence and presence of different concentrations of DSAE, (b) The equivalent circuit model used to fit the experimental impedance data.

In order to obtain information about the kinetics of interfacial mass transfer processes for C-steel corrosion, electrochemical impedance measurements were undertaken in Red Sea Water, in the absence and presence of different concentrations of DSAE. The recorded EIS measurements are presented in Fig. 8a and Table 6.

Table 6. Electrochemical impedance parameters for C-steel in Red Sea Water in the absence and presence of different concentrations of DSAE.

C_{inh} (v/v%)	EIS parameters								
	R_s (Ω cm^2)	Q_f (μS s^{-n} cm^{-2})	n_1	R_f (Ω cm^2)	Q_{dl} (μS s^{-n} cm^{-2})	n_2	R_{ct} (Ω cm^2)	R_p (Ω cm^2)	$IE_P\%$
0.0	3.088	1348	0.68	265	15.20	0.56	200	465 ± 5.30	-
0.5	3.345	1156	0.67	261	12.45	0.94	341	602 ± 7.20	22.76
1.0	3.298	1074	0.66	144	9.73	0.24	576	720 ± 4.41	35.42
2.5	3.233	1036	0.68	91	6.62	0.52	798	889 ± 7.52	47.69
5.0	3.002	511	0.44	5	4.51	0.83	1272	1277 ± 6.34	63.59
10.0	3.829	269	0.81	0.15	1.78	0.64	1373	1373 ± 9.11	66.13

The results obtained can be illustrated as follows:

➢ The shape of the impedance spectra for the Nyquist plots (Figure 8a) remained the same in the absence and presence of different concentrations of DSAE, indicating that almost no change in the corrosion mechanism occurred due to inhibitor action.

➢ Although the appearance of impedance spectra remained the same, their diameter increased after the addition of DSAE to the corrosive solution. This increase was more pronounced with increasing inhibitor concentration, indicating the adsorption of inhibitor molecules on the metal surface [58].

➢ The impedance spectra were appropriately analyzed by fitting into the equivalent circuit model shown in Fig. 8b. It must be noted that the fitting quality was evaluated by Chi-squared (χ^2) values in the range: $1.9 \times 10^{-3} \leq \chi^2 \leq 3.1 \times 10^{-3}$. The suggested equivalent circuit consists of the following elements:

▪ The resistance of the solution between the metal and the counter electrode, R_s,

▪ The film layer resistance, R_f, in parallel with a film capacitance, CPE$_f$, (Q_f, n_1) and,

▪ The charge transfer resistance, R_{ct}, in parallel with a double layer capacitance, CPE$_{dl}$, (Q_{dl}, n_2).

As shown, the constant phase element (CPE) was used in this model to compensate for non-homogeneity in the system and is defined by two values, Q and n. The impedance of the constant phase element (Z$_{CPE}$) is defined as [59]:

$$Z_{CPE} = \left[Q(j\omega)^n \right]^{-1} \tag{16}$$

Where ω is the angular frequency in rad/s, *n* and Q are the CPE parameters. The exponent *n* has values between -1 and 1. A value of -1 is characteristic of an inductance, a value of 0 represents a resistance, a value of 1 corresponds to a capacitor and a value of 0.5 was assigned to the diffusion phenomena (Warburg impedance).

The electrochemical impedance parameters R_s, R_{ct}, $R_p = R_f + R_{ct}$, Q_f, Q_{dl}, n_1, n_2 and *IE$_P$%* for C-steel corrosion in the absence and presence of different concentrations of DSAE were estimated by ZSimDemo 3.20 software (Table 6). As observed, there was no noticeable change in R_s values both in the absence and presence of inhibitor. The presence and increase of DSAE concentration increased

the values of R_p showing that the inhibition efficiency ($IE_P\%$) increased with concentration increase. Since R_p is inversely proportional to corrosion rate, it can be used to calculate inhibition efficiency. In view of Table 6, the results show that the CPEs, Q_f and Q_{dl}, decrease upon addition and increase of DSAE concentration. The decrease of CPEs with increase in DSAE concentration may be attributed to the formation of a protective layer on the electrode surface [60].

　　PDP plots illustrating the effect of DSAE on anodic and cathodic processes for C-steel corrosion in Red Sea Water are shown in Fig.9.
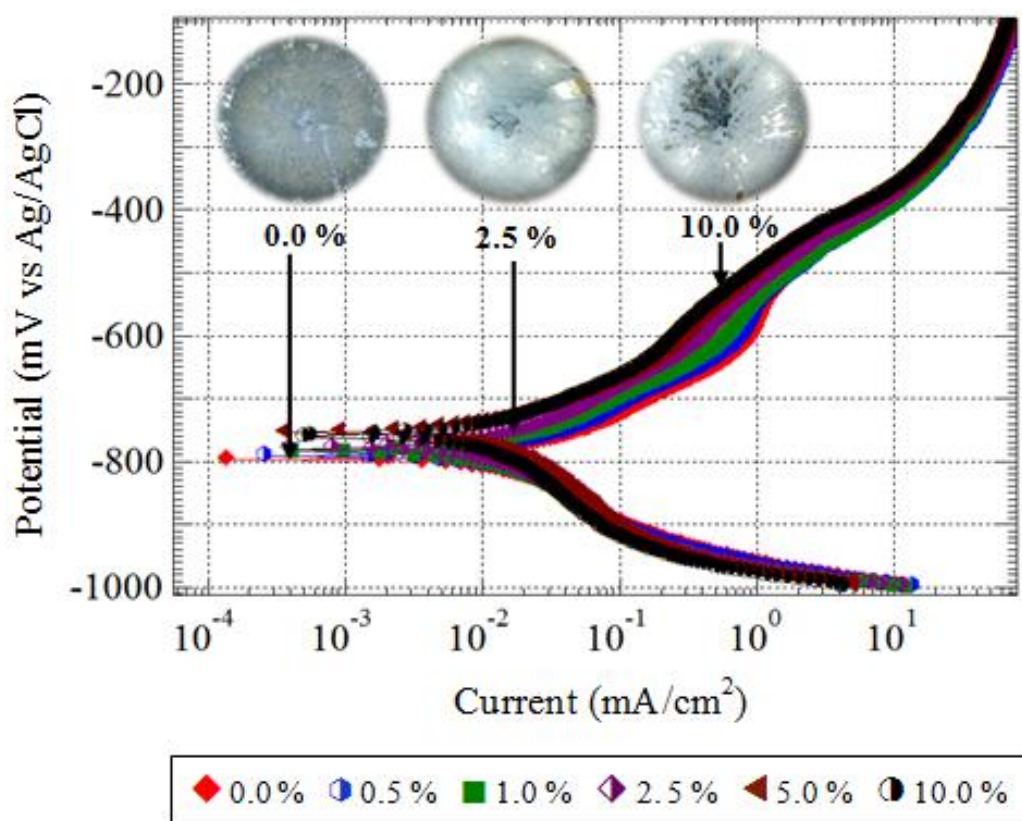
Figure 9. Potentiodynamic polarization curves for C-steel in Red Sea Water in the absence and presence of different concentrations of DSAE.

　　The corresponding polarization parameters such as corrosion potential (E_{Corr}), cathodic and anodic Tafel slopes (β_a and β_c), corrosion current density (i_{corr}) and inhibition efficiency ($IE_i\%$) calculated from i_{corr} values are presented in Table 7. Macroscopic graphs for the working electrode in the absence and presence of DSAE were taken at the end of the polarization experiments (Fig. 9).

Table 7. Potentiodynamic polarization parameters for C-steel in Red Sea Water in the absence and presence of different concentrations of DSAE.

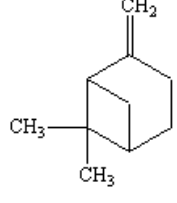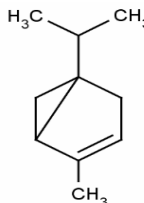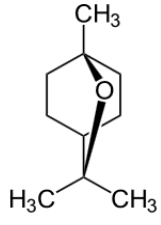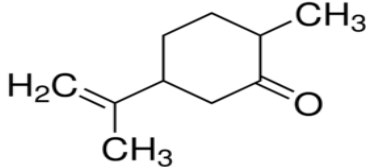| C_{inh} (v/v%)	PDP parameters				
	$-E_{Corr}$ (mV)	β_a (mV dec^{-1})	$-\beta_c$ (mV dec^{-1})	i_{corr} (μA cm^{-2})	$IE_i\%$
0.0	799	80	115	1759 ± 51.40	-
0.5	791	74	107	1464 ± 36.25	16.77
1.0	786	83	109	1359 ± 32.19	22.74
2.5	779	77	109	1141 ± 41.74	35.13
5.0	755	81	114	882 ± 17.27	49.86
10.0	760	77	112	722 ± 11.03	58.95
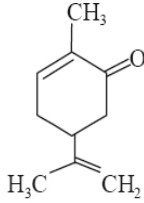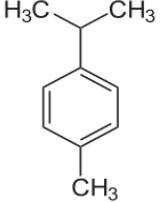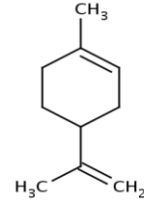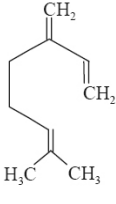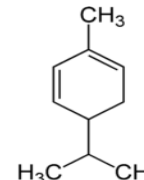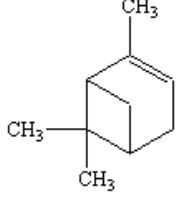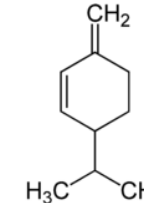
The results can be summarized as follows:

➤ The shapes of the polarization plots for inhibiting solution are not substantially different from that of the uninhibiting solution. The presence of DSAE decreased corrosion rate, but did not alter the mechanism of corrosion. The inhibiting action of DSAE therefore may be related to the adsorption and formation of a barrier film on the electrode surface, thereby protecting it from corrosion.

➤ It is clear from Table 7 that by increasing SDAE concentration, corrosion current density (i_{corr}) decreased and as a result the inhibition efficiency ($IE_i\%$) increased.

➤ The corrosion potential (E_{Corr}) of C-steel shifted to more positive values in DSAE containing solution when compared to solutions without DSAE. This indicates that inhibitor molecules are more adsorbed on anodic sites, resulting in the inhibition of anodic reactions. Generally, if the displacement in E_{Corr} is > 85 mV with respect to E_{Corr} in the uninhibited solution, the inhibitor is said to be cathodic or anodic [61,62]. In our study, the maximum displacement was 44 mV, which indicates that DSAE can be used as a mixed type inhibitor.

➤ In the presence of DSAE, the slight change of both β_a and β_c indicates that the corrosion mechanism of C-steel does not change.

➤ The macroscopic graph in the absence of DSAE shows corrosion on the C-steel surface. This resulted in the formation of small pits and rough surface layers. These observations can be explained on the basis of the presence of aggressive species in the medium such as Cl$^-$ ion and the extent of its contribution to acceleration of metal dissolution [63]. In contrast, the corrosion was dramatically inhibited in the presence of 2.5% and 10.0% of DSAE. The adsorption film effectively protected the C-steel surface from the corrosive medium and this effect increased with increase in DSAE concentration.

3.2.3. Inhibition Mechanism and Inhibitor Constituents

Phytochemical analysis of dill seeds indicated the presence of tannins, glycosides, saponins, steroids, terpenoids, flavonoids, coumarins and reducing sugars [64]. The main constituents of dill seeds are presented in Table 8 [65].

Table 8. Main compounds found in dill seeds.

Name of Compound	Structure	Name of Compound	Structure
d-Carvone		β-Cymene	
d-Limonene		β-Myrcene	
α-Phellandrene		α-Pinene	
β-Phellandrene		β-Pinene	
Thujene		1,8-Cineole	
α-dihydrocarvone			

The content of these main components varies according to geographical origin, harvesting time, growth conditions, and isolation procedure [66].

Adsorption of inhibitor molecules mainly depends on the charge and nature of the metal surface, electronic characteristics of the metal surface, adsorption of solvent and other ionic species, temperature and electrochemical potential at solution interface [67]. The adsorption of inhibitor molecules on metal surface was mainly due to monolayer adsorption (Fig. 10) through the following:

    a. Physical adsorption (physisorption) resulting from electrostatic attraction between inhibiting organic ions or dipoles and the electrically charged metal surface or,

    b. Chemical adsorption (chemisorption) resulting when charge sharing or charge transfer occurs between adsorbates and metal surface atoms, to form a covalent bond or,

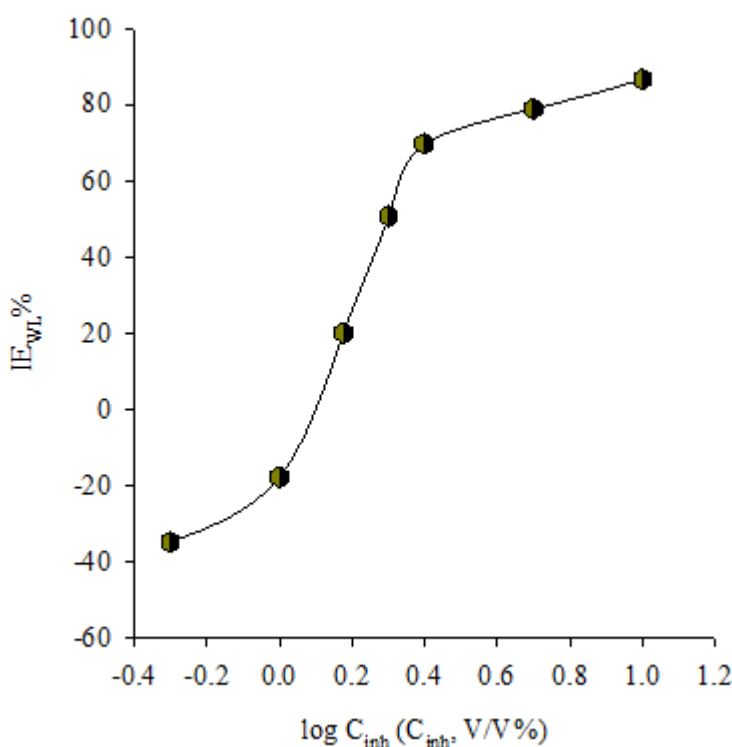   c. Combination of both types of adsorption.

Figure 10. Variation of inhibition efficiency (*IE$_{WL}$%*) with logarithmic concentration of DSAE.

Adsorption of the main constituents of DSAE can be attributed to the presence of O-atoms, π- electrons and aromatic rings. It is a well-established fact that chloride ions being adsorbed on metal surface, promote the adsorption of positively charged ions on metals, by making a bridge between cations and positively charged metals [68]. It is possible that the inhibitor molecules (protonated form of organic moieties) interacted with the steel surface through the aforementioned mechanism and formed a layer at the metal-sea water interface (physisorption); hence, corrosion of steel was inhibited in sea water. In addition, it is possible that the layer at the metal-sea water interface was formed due to

donor-acceptor interactions (chemisorption) between the π electrons or lone pair electrons (from O atoms or aromatic rings of organic moieties) and the vacant ''d'' orbitals of iron surface atoms [69,70].

3.2.4. Effect of Inhibitor on Microbial growth

It is well known that microbes can cause corrosion of metals in different natural environments [71,72, 26]. These microbes and their metabolite products affect the corrosion of metals and consequently damage metal construction and other structures in sea water, resulting in economic losses [71]. Figs.11 & 12 show the microbial counts in two different agar plates (nutrient and *thiobacillus*) for corrosion products formed on C-steel surface after five weeks of immersion in sea water, in the absence and presence of different concentrations of DSAE. The results revealed that DSAE inhibited microbial growth in both agar plates. The microbial growth inhibition increased with increasing DSAE concentration, except at low concentration (0.5% V/V), where microbial growth was accelerated. The inhibition percentage of DSAE on microbial growth is shown in Table 9.
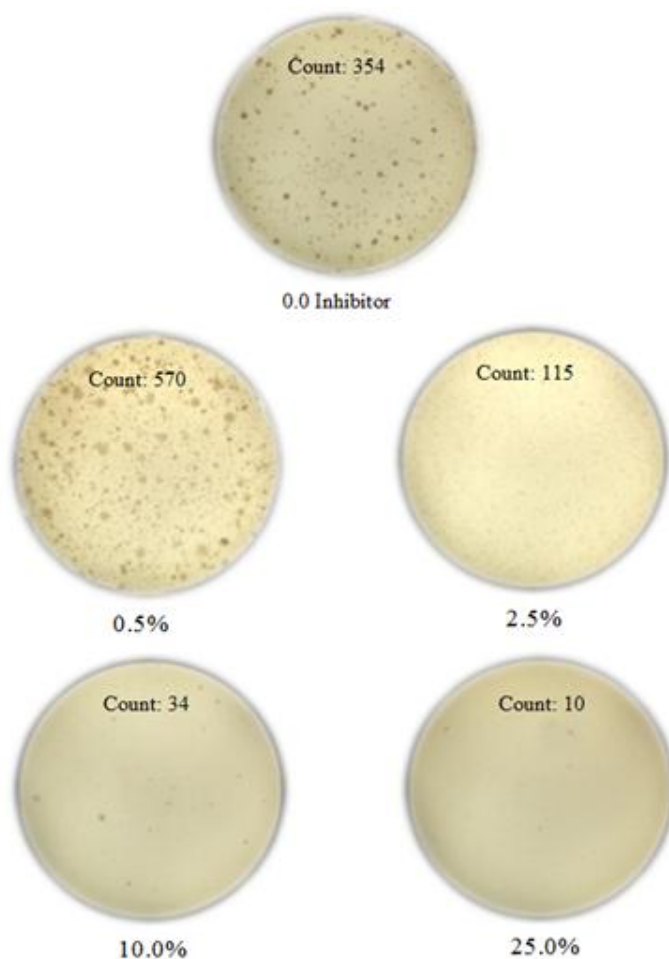

Figure 11. Microbial growth in nutrient agar plates in the absence and presence of different concentrations of DSAE.
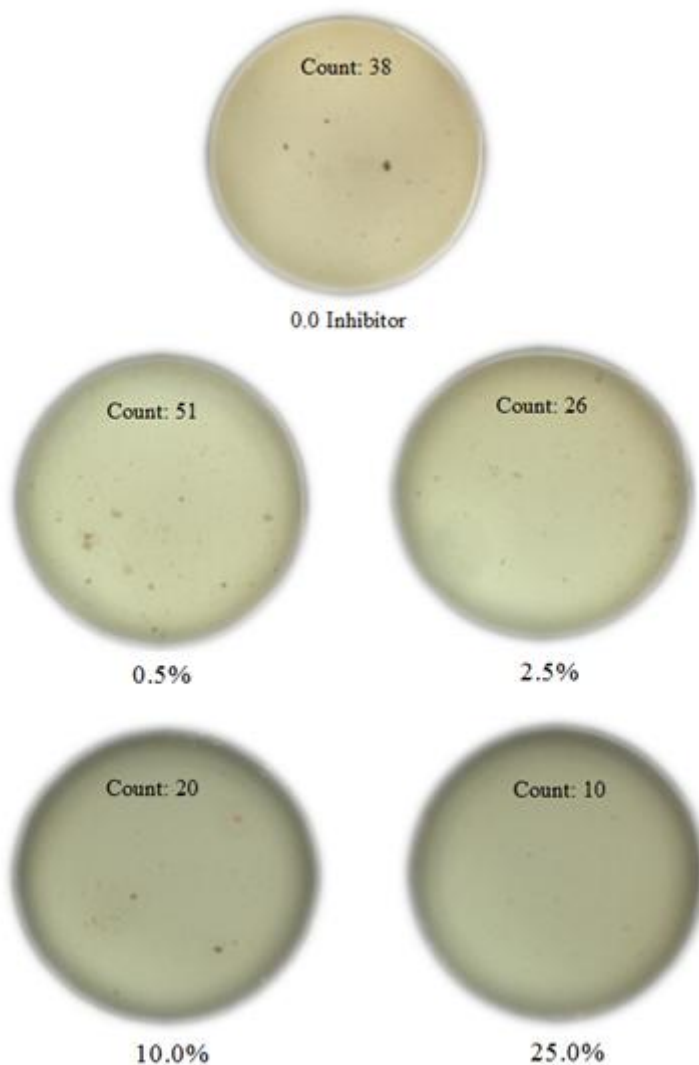
Figure 12. Microbial growth in *thiobacillus* agar plates in the absence and presence of different concentrations of DSAE.

Table 9. Inhibition percentage of DSAE on microbial growth from corrosion products of C-steel in Red Sea Water.

C_{inh} (V/V%)	Inhibition percentage %	
	Nutrient agar plate	***Thiobacillus* agar plate**
0.0	-	-
0.25	-61.02	-34.21
2.5	67.51	31.58
10.0	90.40	47.37
25.0	97.18	73.68

These results are in line with the previous results obtained from weight loss studies of corrosion inhibition, especially at low concentrations. Earlier studies on essential oil of dill revealed its antimicrobial potential [73,74]. The antimicrobial activity of dill against *Escherichia. coli*, *Salmonella*

typhi, *Bacillus subtilis* and *S. aureus*, were reported by Badar *et al.,* [75]. The inhibitory effect of dill on microbes is due to presence of carvone and limonene. In moist environment, d-carvone and d-limonene, are readily oxidized to carveol, carvone and limonene oxide. These products increase production of reactive oxygen species on the surface of microbial tissues, making a little activity for it [76].

4. CONCLUSION

The effect of immersion time and inhibitor concentration on the corrosion behavior of C-steel in Red Sea Water was studied using chemical and electrochemical techniques. The following points were deduced from this investigation:

- The results show that weight loss of C-steel (expressed as pit depth) varied with time according to the power-law equation.
- Kinetic parameters indicate that the corrosion of C-steel occur under mixed control of diffusion and charge transfer processes.
- Macroscopic observations of C-steel in Red Sea Water showed the development of corrosion forms and corrosion products with time.
- DSAE was found to be an effective inhibitor of C-steel corrosion in Red Sea Water. The inhibition efficiency increased with increase in DSAE concentration until a 10% concentration was achieved (optimal concentration) after which the inhibition efficiency started to decrease.
- Electrochemical measurements revealed that DSAE acts as a mixed-type inhibitor without altering the mechanism of C-steel dissolution.
- Good correlation between inhibitor constituents and inhibition efficiency in Red Sea Water was obtained and discussed.
- The effect of DSAE concentration on microbial growth indicates that the antimicrobial properties of DSAE increased with concentration.

References

1. P. R. Roberge, *Handbook of Corrosion Engineering*, McGrow Hill, New York (2000).
2. M. Schumacher, *Seawater Corrosion Handbook*, Park Ridge, New Jersey (1979).
3. D. Aylor, Seawater, In: Baboian R, (Ed.) *Corrosion Tests and Standards: Application and Interpretation*, Pennsylvania, MNL 20, ASTM International (1995).
4. E. Bardal, *Corrosion and Protection: Engineering Materials and Processes*, Springer, London (2004).
5. A.U. Malik, S. Ahmad, I. Andijani, S. Al-Fouzan, *Desalination*, 123 (2-3) (1999) 205.
6. R. E. Melchers, R. Jeffrey, *Corros. Sci.*, 47 (2005) 1678.
7. H. Möller, E. T. Boshoff, H. Froneman, *The Journal of The South African Institute of Mining and Metallurgy*, 106 (2006) 585.
8. S. A. Al-Fouzan, A. U. Malik, *Desalination*, 228 (1-3) (2008) 61.
9. Y. Zou, J. Wanga, Y.Y. Zheng, *Corros. Sci.*, 53 (2011) 208.
10. "Red Sea", Retrieved 6 January (2009).

11. B. Mabrook, *Desalination*, 97 (1994) 453.
12. H. Yu, J. H. Wu, H. R. Wang, J. T. Wang, G. S. Huang, *Corros. Eng. Sci. Technol.*, 41 (3) (2006) 259.
13. F. O. Aramide, *Leonardo Journal of Sciences*, 15 (2009) 47.
14. B-Y. Liu, Z. Liu, G-Ch. Han, Y-H. Li, *Thin Solid Films*, 519 (2011) 7836.
15. V. Johnsirani, J. Sathiyabama, S. Rajendran, A. Suriya Prabha, *International Scholarly Research Network*, 2012 (2012) 1.
16. V. Sribharathy, S. Rajendran, J. Sathiyabama, *Chem. Sci. Trans.*, 2 (1) (2013) 315.
17. E. Nasir, A. I. Ali, *Flora of West Pakistan*, No. 20 Umbelliferae, Stewart Herbarium Gordon College Rawalpindi (1972).
18. G. J. Kaur, D. S. Arora, *BMC Complement. Altern. Med.*, 9 (2009) 30.
19. APHA, AWWA, WEF. *Standard Methods for the Examination of Water and Wastewater*, 21st Ed., American Public Health Association, Washington DC (2005).
20. ASTM G-90, *Standard Practice for Preparing, Cleaning and Evaluating Corrosion Test Specimens* (1990).
21. R. M. Maier, I. L. Pepper, C. P. Gerba, *Environmental microbiology*, 2nd Ed., ELSEVIER (2009).
22. E.Y. Bridson, *The OXOID MANUAL*, 8th Ed. (1998).
23. N. G. Rojas-Avelizapa, M. Gómez-Ramírez, R. Hernández-Gama, J. Aburto, R. García de León, 3rd International Symposium on Environmental Management, *SEM–Towards Sustainable Technologies* (SEM2011), 27 (1) (2013) 109.
24. Y. Zou, J. Wanga, Y. Y. Zheng, *Corros. Sci.*, 53 (2011) 208.
25. M. Natesan, G. Venkatachari, N. Palaniswamy, *Corros. Sci.*, 48 (2006) 3584.
26. E. A. Noor, *Mater. Corros.*, 61 (9999) (2010) 1.
27. E. Bardal, *Corrosion and Protection*, Springer-Verlag London Limited, London (2004).
28. G. Tammann, *Lehrbuch der Metallographie*, 2nd Ed., Leipzig (1923).
29. F. Booth, *Trans. Faraday. Soc.*, 44 (1948) 796.
30. U. R. Evans, *The Corrosion and Oxidation of Metals: Scientific Principles and Practical Applications*, Edward Arnold (Publishers), London (1960).
31. M. Romanoff, *Underground Corrosion*, National Bureau of Standards Circular 579, US Government, Printing Office, Washington DC (1957).
32. Y. Katano, K. Miyata, H. Shimizu, T. Isogai, *Corrosion*, 59 (2) (2003) 155.
33. M. Benarie, F.L. Lipfert, *Atmos. Environ.*, 20 (10) (1986) 1947.
34. M. Morcillo, J. Simancas, S. Feliu, (In) *Atmospheric Corrosion*, ASTM STP 1239 (1995) 195.
35. G. Englehardt, D. D. MacDonald, *Corrosion*, 54 (6) (1998) 469.
36. R. Jeffrey, R. E. Melchers, *Corros. Sci.,* 49 (2007) 2270.
37. T. Misawa, K. Hashimoto, S. Shimodaira, *Corros. Sci.*, 14 (1974) 131.
38. M. R. Gilberg, N. J. Seeley, *Stud. Conserv.,* 26 (1981) 50.
39. S. Pineau, R. Sabot, I. Quillet, M. Jeannin, Ch. Caplat, I. Dupont-Morral, Ph. Refait, *Corros. Sci.*, 50 (2008) 1099.
40. G. Wranglen, *International Conference on Localized Corrosion*, Williamsburg, VA, USA, Dec. 6-10 (1971) 462.
41. R. E. Melchers, *Bioelectrochemistry,* 97 (2014) 89.
42. D.A. Jones, *Principles and Prevention of Corrosion*, 2nd Ed., Prentice-Hall, Upper Saddle River, NJ (1996).
43. J. R. Baylis, *J. Am. Water Works Assoc.,* 15 (6) (1926) 598.
44. L. Daniels, B. Negash, B. S. Rajagopal, P. J. Weimer, *Science,* 237 (4814) (1987) 509.
45. W. H. Lorowitz, D. P. Jr. Nagle, R. S. Tanner, *Environ. Sci. Technol.*, 26 (8) (1992) 1606.
46. S. M. Gravano, J. R. Galvele, *Corros. Sci.,* 24 (6) (1984) 517.
47. Y. Waseda, S. Suzuki, *Characterization of Corrosion Products on Steel Surfaces*, (Eds.), Springer, Berlin (2006).

48. L. L. Shrier, R. A. Jarman, G. T. Burstein, *Corrosion*, Vol. 1, 3rd Ed., Butterworth-Heinemann, Oxford (1994).
49. S. M. Sharland, P. W. Tasker, *Corros. Sci.*, 28 (6) (1988) 603.
50. K. Asami, M. Kikuchi, *Corros. Sci.*, 45 (2003) 2671.
51. Ph. Refait, JM-R. Genin, *Corros. Sci.*, 39 (3) (1997) 539.
52. C. Remazeilles, Ph. Refait, *Corros. Sci.*, 49 (2007) 844.
53. Q. Bai, Y. Zou, J. Wang, L. Zhang, X. Kong, *Adv. Mater. Res.*, 399-401 (2012) 166.
54. A. Turnbull, *Brit. Corr. J.*, 4 (1993) 297.
55. W. A. Hamilton, *Annu. Rev. Microbiol.*, 39 (1985) 195.
56. J-L. Crolet, *From Biology and Corrosion to Biocorrosion*, in: Sequeira, CA, Tiller AK. Eds., Microbial Corrosion, the Institute of Metals, London (1992).
57. O. L. Jr. Riggs, *Corrosion Inhibitors*, 2nd Ed., by C. C. Nathan, NACE, Houston, TX (1973).
58. I. Ahamad, R. Prasad, M. A. Quraishi, *J. Solid State Electrochem.*, 14 (2010) 2095.
59. A. M. Abdel-Gaber, B. A. Abd-El-Nabey, M. Saadawy, *Corros. Sci.,* 51 (2009) 1038.
60. E. McCafferty, N. Hackerman, *J. Electrochem. Soc.*, 119 (1972) 146.
61. E. S. Ferreira, C. Giancomelli, F. C. Giancomelli, A. Sinelli, *Mater. Chem. Phys.*, 83 (2004) 129.
62. W. H. Li, Q. He, S. T. Zhang, C. L. Pei, B. R. Hou, *J. Appl. Electrochem.,* 38 (2008) 289.
63. R. J.Chin, K. Nobe, *J. Electrochem. Soc.,* 119 (1972) 1457.
64. P. Dahiya, Sh. Purkayastha, *Asian Journal of Pharmaceutical and Clinical Research*, **5** (2) (2012) 62.
65. J. E. Simon, L. E. Craker, A. F. Chadwick, *Herbs an Indexed Bibliography*, 1971-1980, The Scientific Literature on Selected Herbs and Aromatic and Medicinal Plants of the Temperate Zone, Archon Books, Hamden, Connecticut (1984).
66. A. A. Koedam, J. J. Scheffer, A. B. Svendsen, *Chem. Mikrobiol. Technol. Lebensm.*, 6 (1976) 1.
67. A. K. Singh, S. K. Shukla, M. Singh, M. A. Quraishi. *Mater. Chem. Phys.*, 129 (2011) 68.
68. A. Khamis, M. M. Saleh, M. I. Awad, *Corros. Sci.*, 66 (2013) 343.
69. X. Li, Sh. Deng, H. Fu, *Corros. Sci.,* 62 (2012) 163.
70. A. Singh, Y. Lin, W. Liu, D. Kuwanhai, E. E. Ebenso, J. Pan, *Int. J. Electrochem. Sci.*, 8 (2013) 12851.
71. X. Li, J. Wang, X. Liu, W. Wang, L. Yan, *Eng. Life Sci.,* 4 (4) (2004) 358.
72. A. Al-Judaibi, A. Al-Moubaraki, *Advances in Biological Chemistry*, 3 (2013) 264.
73. K. K. Aggarwal, S. P. S. Khanuja, A. Ahmad, T. R. S. Kumar, V. K. Gupta, S. Kumar, *Flav. Fragr. J.,* 17 (2001) 59.
74. J. D. Pascal, K. Stanich, B. Girard, G. Mazza, *Int. J. Food Microbiol.,* 74 (2002) 101.
75. N. Badar, M. Arshad, U. Farooq, *Int. J. Agri. Biol.*, 10 (2008) 329.
76. Z. Yu, W. Wang, L. Xu, J. Dong, Y. Jing, *Asian Journal of Traditional Medicines*, 3 (2008) 134.